IEEE Access
Multidisciplinary | Rapid Review | Open Access Journal

Received May 30, 2017, accepted June 24, 2017, date of publication July 11, 2017, date of current version July 31, 2017.

Digital Object Identifier 10.1109/ACCESS.2017.2724601

Enhanced System Acquisition for NB-IoT

WENJIE YANG[1], MIN HUA[1], JINGJING ZHANG[1], TINGTING XIA[1], JUN ZOU[1], CHENGLING JIANG[2], AND MAO WANG[3]

[1]Wireless Networking and Mobile Communications Group, School of Electronic and Optical Engineering, Nanjing University of Science and Technology, Nanjing 210094, China
[2]Information and Telecommunication Branch, State Grid Jiangsu Electric Power Company, Nanjing 210024, China
[3]National Mobile Communications Research Laboratory, Southeast University, Nanjing 211111, China

Corresponding author: Wenjie Yang (wj_yang@njust.edu.cn)

This work was supported in part by the Open Research Fund (2017B01) of the National Mobile Communications Research Laboratory, Southeast University, and in part by the Fundamental Research Fund for the Central Universities under Grant 30920140122005 and Grant 30917011318.

ABSTRACT Machine-type communication (MTC) is the key technology to support data transfer among devices (sensors and actuators) in Internet of Things (IoT). Although cellular communication technologies are developed mainly for ''human-type'' communications, enabling MTC with cellular networks not only improves the connectivity, accessibility, and availability of an MTC network but also has the potential to further drive down the operation cost. However, cellular MTC, especially when applied to low-power massive IoT (mIoT), poses some unique challenges due to the low-cost and low-power nature of an mIoT device. One of the most challenging issues is providing a robust way for an mIoT device to acquire the network under a large frequency offset due to the use of low-cost crystal oscillators and under extended coverage. Although differentiation is a well-known technique for removing impairments caused by frequency offset, its ''noise amplification'' effect limits its applications in cellular communications due to the fact that cellular communication is typically interference limited. Matched-filter-based detection is, therefore, almost unexceptionally used. We show that the differential technique can actually benefit system acquisition in mIoT, where the use of low-cost crystals is a default. Although the existing system acquisition design in a cellular mIoT system, i.e., NB-IoT, facilitates both techniques, there still remain issues that need to be solved in order to take full advantage of the design. We provide a comprehensive analysis on the performance of two most common techniques when applied in a typical NB-IoT environment based on two factors, the geometry factor and the frequency offset factor. Finally, we derive the operating regions for matched-filter-based detection and differentiation using these two factors, in which the system acquisition performance of the two types of techniques is maximized for NB-IoT.

INDEX TERMS Cellular machine-type communications, system acquisition, NB-IoT, low-power massive Internet-of-Things.

I. INTRODUCTION

Internet-of-Things (IoT) enables the objects to exchange information on a massive and global scale [1]. There are a myriad of applications with low requirements on data rate and time delay, such as smart cities, metering, and remote sensing, whose connectivity is powered by machine-type communications (MTC) that are characterized by low power, long battery life (e.g., 10 years or more), wide coverage, and support for devices on a massive scale (hence they must be low cost to manufacture) [2]. The competition in technologies of this category is becoming intense.

In response to the challenges from other technologies (e.g., the proprietary systems like Ultra Narrow Band by SIGFOX [3], LoRa by Semtach [4]) in this growing low-power massive IoT (mIoT) market and the pressure from the cellular providers, recently (September 2015), the 3rd Generation Partnership Project (3GPP) started a work item to standardize a new air-interface, known as Narrow-Band IoT or NB-IoT [5]–[8] for short, operating on a 180-kHz bandwidth (the bandwidth of an LTE resource block (RB) for both downlink and uplink), to enable the power and spectrally more efficient operation of MTC in the bands that are narrower than the minimum LTE system operating bandwidth (1.08 MHz), particularly in the 200-kHz GSM bands. This design achieves great coexistence performance with GSM and LTE system. NB-IoT also establishes the foundation of a new solution for mIoT, which will be an important integral part of the fifth generation (5G) systems

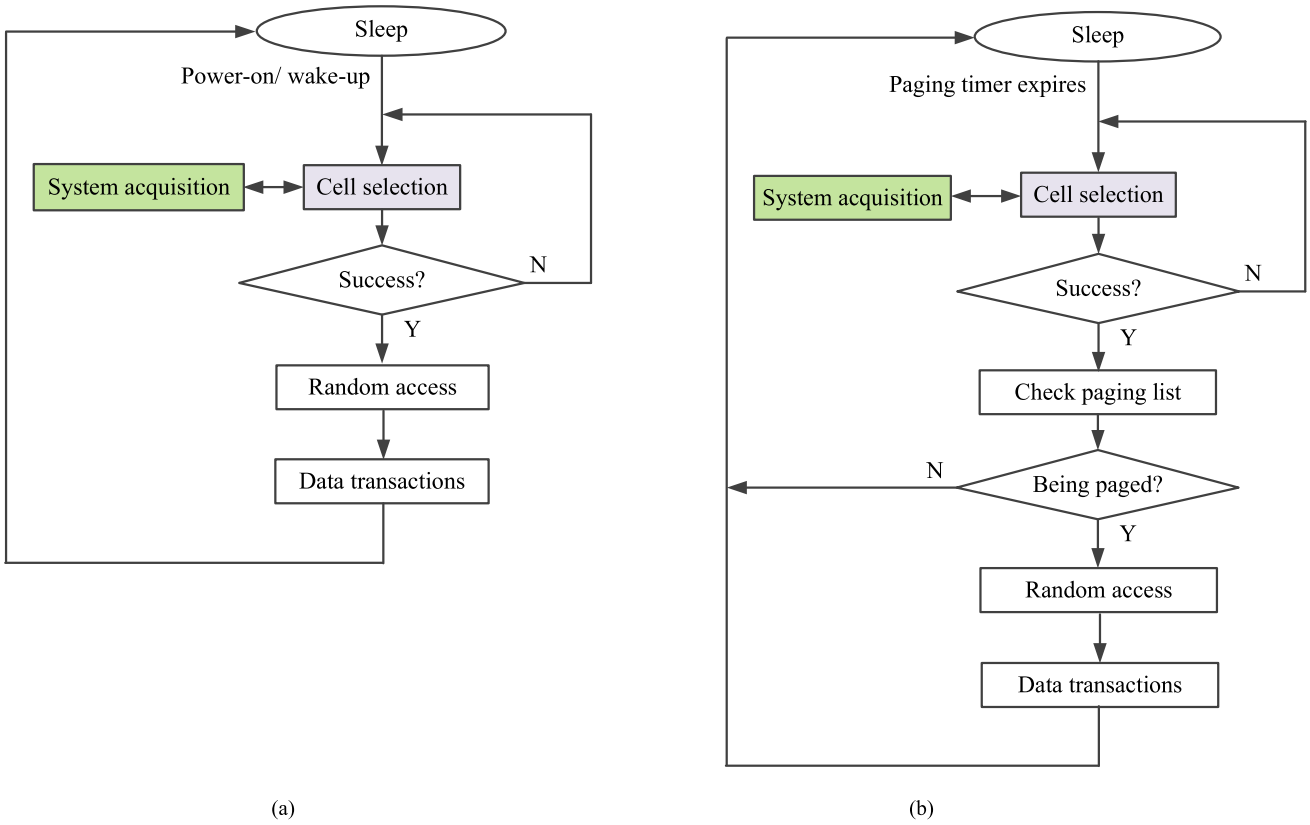

FIGURE 1. Typical operations involved in device-originated (power up or in response to higher layer data transfer request) and network-originated (paging) calls. (a) Device-originated calls. (b) Network-originated calls.

in the future [9]–[11]. The core specifications of NB-IoT were finished in June 2016, and the commercial launch is expected to be initiated in 2017. Due to the extreme short time for development, NB-IoT reused most part of the LTE air interface.

Nevertheless, the greatest challenge that cellular MTC faces is the large discrepancy (in transceiver properties and applications) between the NB-IoT device and the LTE user equipment (UE) for human-type communications (HTC). Among those, low cost of production, deployment, and maintenance is one of the most important aspects of NB-IoT devices so that they can be deployed on a mass scale and even in a disposable manner, contrasting the high-cost nature of the LTE UE. Consequently, the transceiver performance may be impaired, and certain cellular operations, like initial system acquisition, designed for a regular LTE UE, may not function well under certain circumstances.

The purpose of this paper is to analyze the impact of the frequency offset on the initial system acquisition caused by an inaccurate crystal oscillator with a focus on the low-power mIoT system, in particular NB-IoT. We investigate the behavior of different acquisition techniques, i.e., the matched-filter technique and the differentiation technique, under NB-IoT operating conditions, and we show that the detection performance is governed by two factors introduced in this paper: the geometry factor and the frequency offset factor. The contribution of this paper is thus to show that the matched-filter detector precedes the differential detector in performance when geometry factor prevails and the differential detector becomes superior when frequency offset factor dominates. According to the actual operating condition, i.e., the dominance of the two factors, the device can thus select the right detector so that the immunity to both frequency offset and low signal quality can be maximized.

Section II gives a brief description of the system acquisition procedure and points out the challenges of the synchronization signal detection in NB-IoT. In Section III, we analyze the detection performance of two detection techniques, i.e., a traditional matched-filter based detection and a differential detection. Section III also makes a comparison of these two techniques and addresses their limitations respectively when applied to NB-IoT. Based on the analysis results, Section IV derives the operating regions for these two techniques, thereby enabling a device to select a detector accordingly to increase the frequency offset immunity of a device in an NB-IoT environment. Section V concludes this paper.

II. SYSTEM ACQUISITION AND FREQUENCY OFFSET IN NB-IoT

Fig. 1 shows typical operations performed by an NB-IoT device during power-up or wake-up in response to a data transfer request (e.g., meter reporting) or paging timer

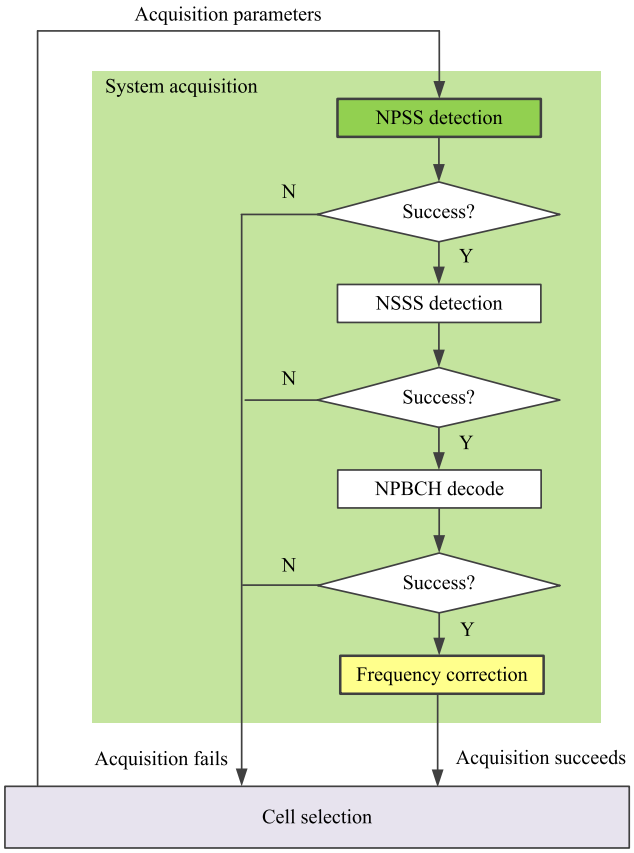

FIGURE 2. Flowchart of the NB-IoT system acquisition.

expiration. Upon waking up, the device obtains the system acquisition information from the cell selection protocol that maintains a list of most recently used (MRU) cells. In the case that none of the cells in the list can be found or in the case of the first time power-up, the device performs a full frequency scan looking for a new cell or system at a frequency raster of, e.g., 100 kHz. To simplify the search, the cell selection protocol also maintains a list of the candidate systems and their associated acquisition information provided by the operator, commonly referred to as a preferred roaming list or PRL [12]. In either case, whether the device is looking for a cell in the current system or an entirely new system, it must first perform the system acquisition procedure as shown in Fig. 2. The device searches for the downlink synchronization signals, e.g., a narrowband primary synchronization signal (NPSS) and a narrowband secondary synchronization signal (NSSS) in NB-IoT system, at the raster frequency to detect the presence of a cell at this frequency and acquire the accurate timing and frequency of the system, e.g., the symbol and frame timing, carrier frequency, and sampling clock. The device can then decode the system information block transmitted on the downlink broadcast channels (e.g., narrowband physical broadcast channel (NPBCH) in NB-IoT) and obtain the system information necessary for establishing a communication link with the system [13], [14]. A failed detection (i.e., a miss) of the synchronization signal may trigger a full frequency re-scan, thereby incurring excessive power consumption and, consequently, a shortened battery life.

Most mIoT applications are characterized by bursty low rate transmissions. The size of data involved in each transaction is typically small. For example, a few transmissions a day and several kilobytes per transmission is typical for an automated water meter. Assuming 1 kilobyte per report, the data transmission takes $\sim$32 subframes (i.e., 32 ms). The NPSS detection thus may account for at least 10 ms/(10 + 32) ms =24% of the total power consumption considering that the NPSS detection takes at least 10 ms to accomplish one search. System acquisition thus becomes a significant part of the total power consumption per wakeup. Therefore, it is a key factor of an mIoT system, and cannot be overlooked in the overall system design.

The challenge of the detection of the synchronization signal lies in the fact that (1) the device has no knowledge about the system timing, and (2) the local frequency of the device is not yet synchronized to the network, after waking up from a sleep, especially, during initial power-on or after a long sleep, and a large offset/error may exist between the device and the network. These large time and frequency uncertainties seriously impair the acquisition performance.

The frequency offset between the device and the network is determined by the accuracy and stability of the local ''free-running'' crystal oscillator of an NB-IoT device. The offset is thus the deviation of the oscillator frequency from the specified target frequency (i.e., the cellular network carrier frequency). Factors such as temperature, crystal aging, and vibration affect the frequency accuracy and stability of the crystal. Among these, temperature is the primary factor that affects the accuracy, and hence needs to be compensated in practice.

The offset (without compensation) typically ranges from $\pm$5 ppm to $\pm$100 ppm (or $\pm$5 kHz to $\pm$100 kHz at 1- GHz carrier frequency) depending on the quality of the crystal. For a low-cost NB-IoT device, the initial frequency error could be well above $\pm$5 ppm (e.g., $\pm$20 ppm or $\pm$20 kHz at 1-GHz carrier frequency), especially for the very first initial system acquisition when the local crystal oscillator is never synchronized to the network (i.e., no compensation/correction has ever been made). Since the frequency accuracy of a crystal depends heavily on temperature, a cellular HTC device is thus typically equipped with a temperature-compensated crystal (TCXO). Not only is a TCXO costly but also power consuming to maintain, which is a luxury that a typical NB-IoT device cannot afford. Clearly, the system acquisition for an NB-IoT device is more challenging than that for an HTC device (e.g., LTE UE). Therefore, one of the key issues in NB-IoT is efficient detection of the synchronization signal under potentially large frequency offset.

Besides, there is a substantial market for the mIoT use cases in which devices are deployed deep inside a building (e.g., in the basement), which requires coverage enhancement over the current LTE cell footprint (maximum coupling

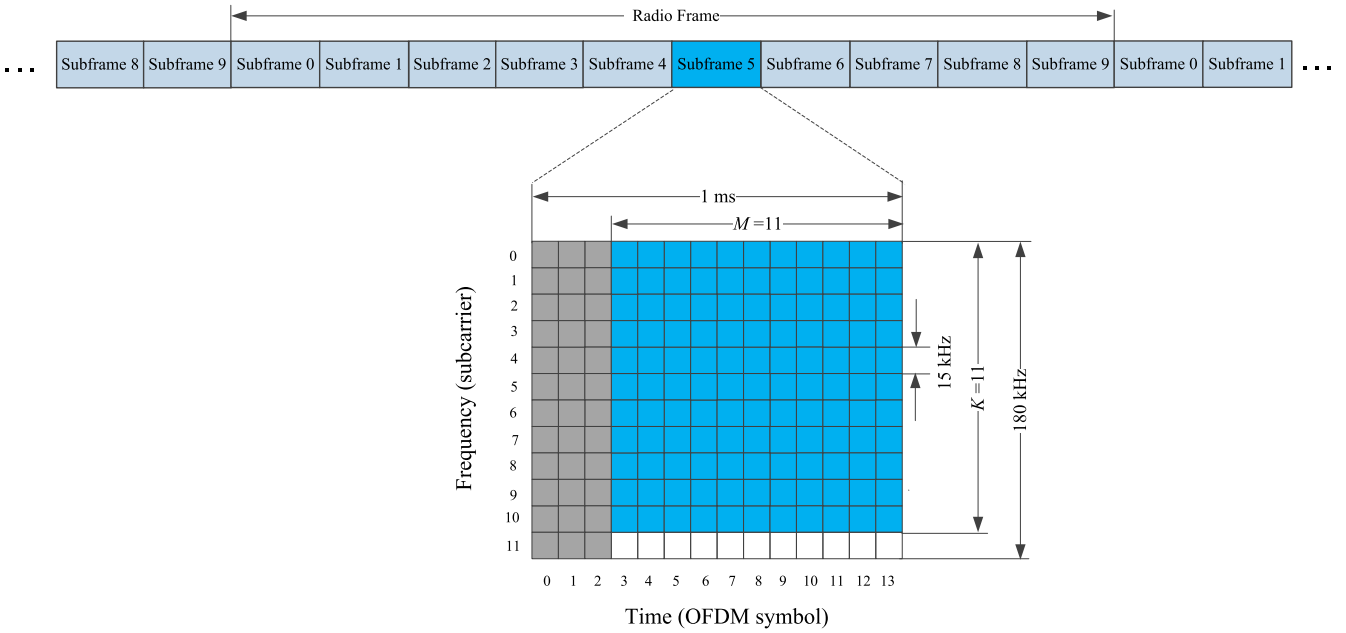

FIGURE 3. Illustration of the narrowband primary synchronization signal (NPSS) resource allocation in an NB-IoT system.

loss of 144 dB). A coverage extension of 20 dB for NB-IoT is hence targeted to increase the coverage to areas where NB-IoT devices are potentially deployed [2]. This extension provides the cellular network with the ability to support devices in locations with excessive penetration losses, where the traditional cellular system has difficulty to reach. Thus, another unique challenge for synchronization signal detection lies in the reduced signal quality due to the coverage extension requirement in NB-IoT.

The downlink synchronization signals in NB-IoT consist of two periodically-broadcast signals: an NPSS and an NSSS. NPSS serves the purpose of providing initial timing and frequency information; and NSSS is for timing and frequency refinement (among other things) under much less time and frequency ambiguities. Clearly, the detection of NPSS is performed under the largest time and frequency ambiguities, and is hence the most challenging part of the overall system acquisition, and ergo the focus of this paper.

III. NPSS DETECTION WITH FREQUENCY OFFSET

The generation of an NPSS waveform is from the frequency domain sequence using the $K = 11$ subcarriers (out of 12) of the last $M = 11$ OFDM symbols of Subframe 5, as shown in Fig. 3. It is then transformed into a time-domain waveform (via inverse Fourier transform), and transmitted in each radio frame. Specifically, the time domain waveform can be mathematically expressed as

$$\mathbf{x} = \left[\mathbf{x}_0 \;\; \mathbf{x}_1 \;\; \cdots \;\; \mathbf{x}_m \;\; \cdots \;\; \mathbf{x}_{M-1}\right], \tag{1}$$

where

$$\begin{aligned}\mathbf{x}_m &= c_m \mathbf{s} \\ &= \left\{x_{m,i} = c_m s_i, \quad 0 \le i \le K-1\right\}.\end{aligned} \tag{2}$$

Here $0 \le m \le M-1$ is the OFDM symbol index, $0 \le i \le K-1$ is the time-domain sample index of an OFDM symbol, and

$$\mathbf{s} = \left\{ s_i = \frac{1}{\sqrt{K}} \sum_{k=0}^{K-1} u_k e^{j2\pi \frac{k}{K} i}, 0 \le i \le K-1 \right\} \tag{3}$$

is the NPSS base waveform in time domain, generated from a Zadoff-Chu (ZC) sequence in frequency domain (via an inverse Fourier transform as shown in (3)), occupying the $K = 11$ subcarriers of an OFDM symbol,

$$\left\{u_k = e^{-j\frac{\pi \mu k(k+1)}{K}}, 0 \le k \le K-1\right\}, \tag{4}$$

with $\mu = 5$. Since a prime number ($K = 11$) is required by a ZC sequence [15], [16], the 12^{th} subcarrier is left unused. This base waveform, $\mathbf{s}$, which has a constant amplitude of 1 [17], occupies the duration of one OFDM symbol and is repeated $M = 11$ times covering the last 11 OFDM symbols of Subframe 5 to form the NPSS. On top, an 11-bit sequence, i.e., $\mathbf{c} = [1111-1-1111-11]$, is applied as a cover sequence for the 11 repeated base waveforms to avoid the timing ambiguity as a result of the repetitions. As such, c_m in (2), i.e., the m^{th} element of $\mathbf{c}$, is used as the cover code for the m^{th} repeated base waveform on the m^{th} NPSS OFDM symbol($m = 0, 1, \cdots, 10$).

The received i^{th} sample of the m^{th} base signal of the baseband NPSS by the device with a frequency offset Δf

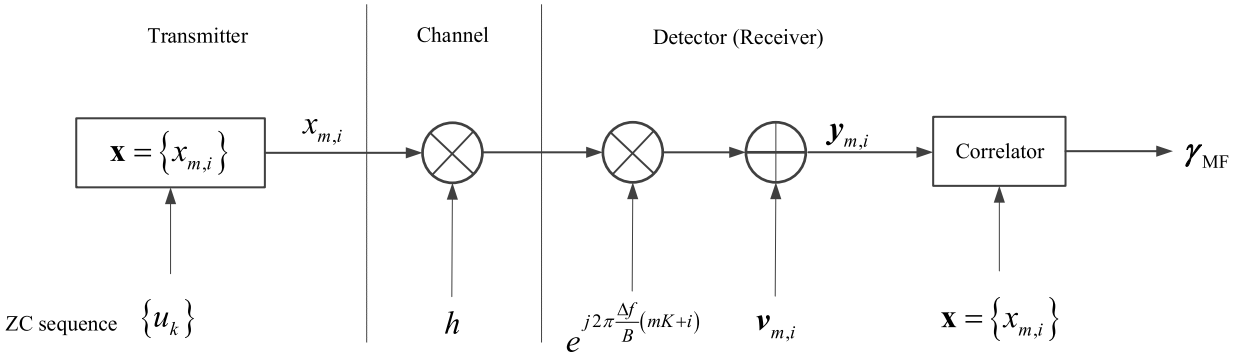

FIGURE 4. A simplified baseband model of a NPSS transceiver, where the transmitter is the base station, and the detector is the NB-IoT device.

between this device and the network (i.e., the base station) can be expressed as

$$\begin{aligned} y_{m,i} &= hx_{m,i}e^{j2\pi\frac{\Delta f}{B}(i+mK)} + v_{m,i} \\ &= hc_m s_i e^{j2\pi\frac{\Delta f}{B}(i+mK)} + v_{m,i}, \quad 0 \le m \le M-1, \\ &\qquad\qquad 0 \le i \le K-1, \end{aligned} \tag{5}$$

where B is the NPSS signal bandwidth, $v_{m,i}$ is the independent zero-mean complex Gaussian noise with variance σ^2, and h is the complex channel gain, unknown but assumed to be constant over the NPSS transmission duration.

The SNR of the received sample $y_{m,i}$ in (5), henceforth referred to as the geometry of the device, is defined as

$$\eta \triangleq \frac{|hx_{m,i}|^2}{E\left\{|v_{m,i}|^2\right\}} = \frac{|h|^2}{E\left\{|v_{m,i}|^2\right\}} = \frac{|h|^2}{\sigma^2}. \tag{6}$$

Geometry is commonly used in the cellular community to indicate the position of a device in a cell. A device located at the center of the cell, i.e., at a high geometry, typically enjoys a high SNR and a device at the edge of the cell, i.e., at a low geometry, suffers from a low SNR. Geometry is interchangeable with received signal SNR in the following discussion.

Based on its unique structure, there are mainly two well-known baseline methods that are best suited for NPSS detection: the matched-filter detection [18]–[20] and the differential detection [21], [22]. Although there are other techniques, they can be considered as variants of these two fundamental techniques.

A. MATCHED-FILTER DETECTION

To detect the presence and timing of a system, a device employs a detector that is essentially a correlator that performs correlation of the received signal at every sample point within a duration whose length equals the period of the NPSS (e.g., 10 ms) against a local copy/template of the NPSS waveform. This correlator is the traditional matched-filter detector, as shown in Fig. 4. In the absence of a frequency error/offset, the largest correlation happens when the local waveform is aligned with the received NPSS signal. When the received NPSS signal is corrupted by noise as shown in (5), the output of the correlator becomes

$$\begin{aligned} \gamma_{\mathrm{MF}} &= \frac{1}{MK}\sum_{m=0}^{M-1}\sum_{i=0}^{K-1}\left(y_{m,i}\cdot x_{m,i}^*\right) \\ &= \frac{1}{MK}\sum_{m=0}^{M-1}\sum_{i=0}^{K-1}\left(hx_{m,i}e^{j2\pi\frac{\Delta f}{B}(i+mK)} + v_{m,i}\right)\cdot x_{m,i}^* \\ &= h\gamma\left(\Delta f\right) + \upsilon, \end{aligned} \tag{7}$$

where $\upsilon \triangleq \frac{1}{MK}\sum_{m=0}^{M-1}\sum_{i=0}^{K-1} v_{m,i}x_{m,i}^* \sim CN\left(0, \frac{\sigma^2}{MK}\right)$, and

$$\gamma\left(\Delta f\right) = e^{j\pi\frac{\Delta f}{B}(MK-1)}\mathrm{sinc}\left(\frac{\Delta f}{B/MK}\right), \tag{8}$$

where

$$\mathrm{sinc}\left(x\right) \triangleq \frac{1}{MK}\cdot\frac{\sin\left(\pi x\right)}{\sin\left(\pi x/MK\right)}, \tag{9}$$

indicating that the received NPSS strength is attenuated by a factor of $|\gamma\left(\Delta f\right)| = \left|\mathrm{sinc}\left(\frac{\Delta f}{B/MK}\right)\right|$, thereby entailing a reduction in the detected NPSS energy by $|\gamma\left(\Delta f\right)|^2$, due to the frequency offset Δf. For instance, a $|\Delta f|$ value about 5 kHz causes a reduction by more than 20 dB (cf. Fig. 5). In order to keep the degradation manageable, $|\Delta f|$ must be well below 5 kHz (i.e., $\Delta f \ll 5$ ppm at 1-GHz carrier frequency), which can be hard to achieve for low-cost NB-IoT devices. It is clear that the optimal matched-filter technique for the synchronization signal detection in the absence of a frequency offset/error, suffers signal energy attenuation in the presence of a high frequency offset between the transmitter and a receiver. Thus, the frequency offset has a profound effect on the performance of NPSS detection for a low-cost NB-IoT device that may have a large frequency offset, especially during the initial system acquisition or after wakeup from a long sleep.

It is worth mentioning that there is an important variant of the baseline matched-filter detector that, instead of using a single local template $\mathbf{x}$ [cf. (1)], this technique consists of H template waveforms, each of which matches to the NPSS

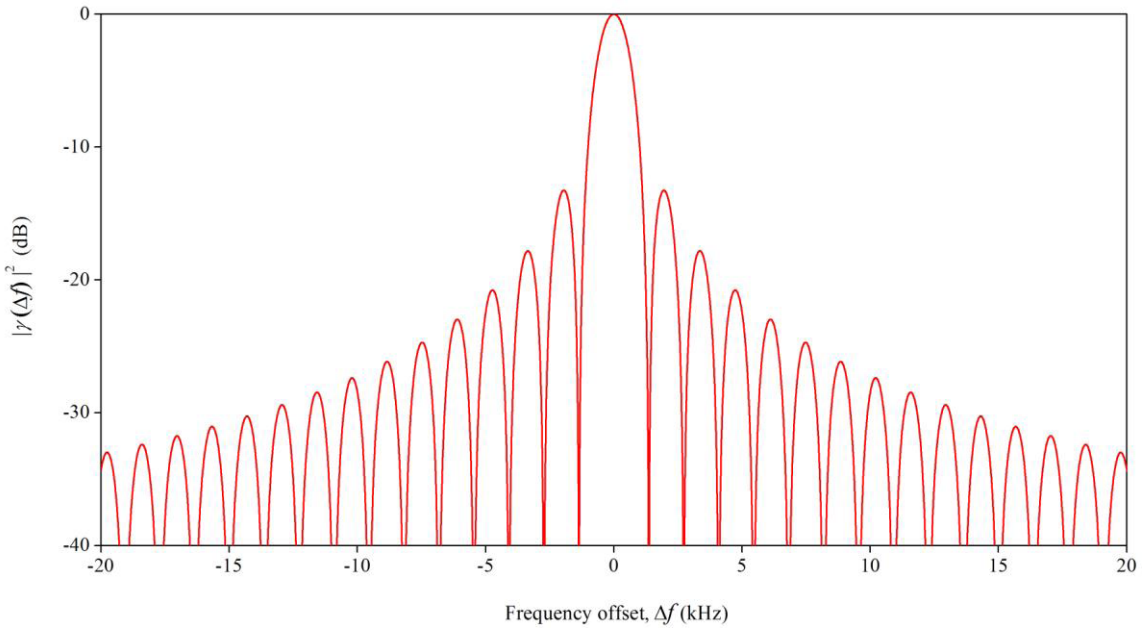

FIGURE 5. Plot of $|\gamma(\Delta f)|^2$ in (8) as a function of frequency offset $\Delta f \in (-20\text{kHz}, 20\text{kHz})$, i.e., ±20 ppm at 1-GHz carrier frequency, to show how frequency offset changes the detection energy.

waveform with a hypothesized frequency offset [23], i.e.,

$$\mathbf{x}^q = \left\{\mathbf{x}_m^q, 0 \le m \le M-1\right\}, \tag{10}$$

where

$$\mathbf{x}_m^q = \mathbf{x}_m \cdot diag\left(e^{j2\pi\frac{\Delta f_q}{B}mK} \quad e^{j2\pi\frac{\Delta f_q}{B}(1+mK)} \quad \cdots \quad e^{j2\pi\frac{\Delta f_q}{B}(K-1+mK)}\right), \tag{11}$$

and Δf_q is the q^{th} $(0 \le q \le H-1)$ hypothesis frequency offset. This variant of matched-filter detector effectively reduces the frequency error range by a factor of H, which helps improve the frequency error immunity of the detector. The only downside of this detector is the linear increase in detection complexity by a factor of H.

B. DIFFERENTIAL DETECTION

Differentiation is a well-known technique for removing the phase component from the received signal, making it a viable technique for mIoT systems. The design of the repeated NPSS structure facilitates the use of such a differential detector to mitigate the effect of large frequency offset [21]. Instead of performing correlation between the received signal and the local copy of the NPSS waveform, the receiver performs piecewise correlation between two adjacent received signals (after the cover code is removed), each of K samples (the length of the base waveform). The output of the correlator reaches a maximum when the correlation is time-aligned with the incoming NPSS, at which the correlation becomes between two received consecutive base waveforms or base signals. The output of the differential correlator between the $(m-1)^{\text{th}}$ received base signal and the m^{th} received base signal is then

$$\begin{aligned}\boldsymbol{\phi}_m &= \frac{1}{K}\sum_{i=0}^{K-1}\left(c_{m-1}\mathbf{y}_{m-1,i}\right)\cdot\left(c_m\mathbf{y}_{m,i}\right)^* \\ &= \frac{1}{K}\sum_{i=0}^{K-1}\left(c_{m-1}hc_{m-1}s_i e^{j2\pi\frac{\Delta f}{B}(i+(m-1)K)} + c_{m-1}\boldsymbol{v}_{m-1,i}\right) \\ &\quad\cdot\left(c_m^*h^*c_m^*s_i^* e^{-j2\pi\frac{\Delta f}{B}(i+mK)} + c_m^*\boldsymbol{v}_{m,i}^*\right) \\ &= |h|^2 e^{-j2\pi\frac{\Delta f}{B}K} + \boldsymbol{w}_m, \quad 1 \le m \le M-1,\end{aligned} \tag{12}$$

where

$$\boldsymbol{w}_m \triangleq \frac{1}{K}\sum_{i=0}^{K-1}\boldsymbol{w}_{m,i}, \tag{13}$$

and

$$\begin{aligned}\boldsymbol{w}_{m,i} &= hs_i e^{j2\pi\frac{\Delta f}{B}(i+(m-1)K)}c_m^*\boldsymbol{v}_{m,i}^* \\ &\quad + h^*s_i^* e^{-j2\pi\frac{\Delta f}{B}(i+mK)}c_{m-1}\boldsymbol{v}_{m-1,i} \\ &\quad + c_{m-1}c_m^*\boldsymbol{v}_{m-1,i}\boldsymbol{v}_{m,i}^*.\end{aligned} \tag{14}$$

Since $\boldsymbol{v}_{m-1,i}$ and $\boldsymbol{v}_{m,i}$ in (14) are mutually independent, $E\left\{\boldsymbol{w}_{m,i}\right\} = 0$, and

$$\begin{aligned}&\text{Var}\left\{\boldsymbol{w}_{m,i}\right\} \\ &= |h|^2\,\text{Var}\left\{s_i e^{j2\pi\frac{\Delta f}{B}(i+(m-1)K)}c_m^*\boldsymbol{v}_{m,i}^*\right\} \\ &\quad + |h|^2\,\text{Var}\left\{s_i^* e^{-j2\pi\frac{\Delta f}{B}(i+mK)}c_{m-1}\boldsymbol{v}_{m-1,i}\right\} \\ &\quad + \text{Var}\left\{c_{m-1}c_m^*\boldsymbol{v}_{m-1,i}\boldsymbol{v}_{m,i}^*\right\} \\ &= |h|^2\,\text{Var}\left\{\boldsymbol{v}_{m,i}^*\right\} + |h|^2\,\text{Var}\left\{\boldsymbol{v}_{m-1,i}\right\} + \text{Var}\left\{\boldsymbol{v}_{m-1,i}\right\} \\ &\quad \cdot \text{Var}\left\{\boldsymbol{v}_{m,i}^*\right\} \\ &= 2|h|^2\sigma^2 + \sigma^4.\end{aligned} \tag{15}$$

The total output can be expressed as

$$\begin{aligned}\boldsymbol{\gamma}_{\mathrm{DIF}} &= \frac{1}{M-1}\sum_{m=1}^{M-1}\boldsymbol{\phi}_m \\ &= |h|^2 e^{-j2\pi\frac{\Delta f}{B}K} + \boldsymbol{\omega}, \end{aligned} \tag{16}$$

where

$$\boldsymbol{\omega} = \frac{1}{M-1}\sum_{m=1}^{M-1}\boldsymbol{w}_m. \tag{17}$$

The differential operation which is the correlation of the adjacent two base signals in (12) results in an output $\left|\boldsymbol{\gamma}_{\mathrm{DIF}}\right| = |h|^2$ that is not a function of Δf, making the detection free of the effect of frequency offset, whereas the matched-filter detector in (7) suffers from a detection energy loss due to the frequency offset.

It seems that the differential detector solves the frequency offset problem. However, it has a new issue as is discussed in detail in the following subsection.

C. DIFFERENTIAL DETECTION VS MATCHED-FILTER DETECTION

Now we look into the issue of the differential detector, i.e., the impact of the differentiation on the detection SNR of the differential correlator.

First, the corresponding detection SNR of the matched-filter detector whose correlator is matched to the original transmitted signal, as shown in Fig. 4, can be represented as

$$\begin{aligned}\zeta_{\mathrm{MF}}(\eta, \Delta f) &= \frac{|h|^2\left|\mathrm{sinc}\left(\frac{\Delta f}{B/MK}\right)\right|^2}{\sigma^2/MK} \\ &= MK\eta\left|\mathrm{sinc}\left(\frac{\Delta f}{B/MK}\right)\right|^2, \end{aligned} \tag{18}$$

when the synchronization signal is present, and in alignment with the local NPSS sequence, i.e., $\mathbf{x} = \left\{x_{m,i}, 0 \le m \le M-1, 0 \le i \le K-1\right\}$.

Next, we look at the effect of differentiation on the output SNR of the correlator of the differential detector. The noise at the output of the detector (16) can be further expressed as

$$\boldsymbol{\omega} = \frac{1}{K(M-1)}\sum_{a=1}^{\frac{M-1}{2}}\sum_{i=0}^{K-1}\boldsymbol{w}_{2a-1,i} + \frac{1}{K(M-1)}\sum_{a=1}^{\frac{M-1}{2}}\sum_{i=0}^{K-1}\boldsymbol{w}_{2a,i}. \tag{19}$$

The terms in each of these two summations of (19) are independent since $E\left\{\boldsymbol{w}_{m_1,i_1}\boldsymbol{w}^*_{m_2,i_2}\right\} = 0\,(m_1 \ne m_2)$, for

$$m_1, m_2 \in N_1 \triangleq \left\{2a \,\middle|\, a = 1, 2, \cdots, \frac{M-1}{2}\right\} \tag{20}$$

or

$$m_1, m_2 \in N_2 \triangleq \left\{2a-1 \,\middle|\, a = 1, 2, \cdots, \frac{M-1}{2}\right\}. \tag{21}$$

For sufficiently large $K(M-1)$, each sum is Gaussian with distribution $CN\left(0, \frac{1}{2K(M-1)}\left(2|h|^2\sigma^2 + \sigma^4\right)\right)$, according to the central limit theorem. Since $\boldsymbol{\omega}$ is the sum of two Gaussians, it is also Gaussian, with zero mean and variance of

$$\sigma^2_{\mathrm{DIF}} = \frac{1}{K(M-1)}\left(2|h|^2\sigma^2 + \sigma^4\right). \tag{22}$$

The detection SNR of the differential detector (16) is thus

$$\zeta_{\mathrm{DIF}}(\eta) = \frac{\left(|h|^2\right)^2}{\frac{1}{K(M-1)}\left(2|h|^2\sigma^2 + \sigma^4\right)} = \frac{K(M-1)}{\frac{2}{\eta} + \frac{1}{\eta^2}}, \tag{23}$$

which is only a function of the device geometry (*not* a function of the frequency offset).

The "noise amplification" factor as a result of the differential operation is then

$$\begin{aligned}\frac{\zeta_{\mathrm{DIF}}(\eta)}{\zeta_{\mathrm{MF}}(\eta, \Delta f)} &= \frac{\frac{M-1}{M}\left(2+\frac{1}{\eta}\right)^{-1}}{\left|\mathrm{sinc}\left(\frac{\Delta f}{B/MK}\right)\right|^2} \\ &= \frac{\varphi(\eta)}{\rho(\Delta f)} \\ &= \varphi(\eta) - \rho(\Delta f)\,(\mathrm{dB}), \end{aligned} \tag{24}$$

where

$$\varphi(\eta) \triangleq \frac{M-1}{M}\left(2+\frac{1}{\eta}\right)^{-1} \tag{25}$$

is a factor related to the device geometry η, referred to as the geometry factor, and

$$\rho(\Delta f) \triangleq \left|\mathrm{sinc}\left(\frac{\Delta f}{B/MK}\right)\right|^2 \tag{26}$$

is the frequency offset factor, a function of the frequency offset. They are plotted in Fig. 6 (a) and Fig. 6 (b). The geometry factor represents the degradation in detection SNR due to the noise amplification effect of differentiation whose degree of attenuation is determined by the device's geometry η, whereas the frequency offset factor also represents the detection SNR degradation, but due to the reduction of the detection energy as a result of the frequency offset between the device and the network.

Clearly, for the frequency offset factor, we have

$$\rho(\Delta f) \le 1\ (0\ \mathrm{dB}), \tag{27}$$

where equality holds when $\Delta f = 0$, and for the geometry factor

$$\varphi(\eta) < \frac{1}{2}\cdot\frac{M-1}{M} < \frac{1}{2}(-3\mathrm{dB}). \tag{28}$$

That is, the output SNR of the differential detector is at least 3 dB lower than the matched-filter detector at low frequency offset ($\rho(\Delta f) = 0\mathrm{dB}$), reflecting the noise amplification effect of differentiation. In the high geometry scenario, i.e., $\eta \gg 5\mathrm{dB}$,

$$\lim_{\eta\to\infty}\varphi(\eta) = \frac{1}{2}\cdot\frac{M-1}{M} < \frac{1}{2}(-3\ \mathrm{dB}), \tag{29}$$

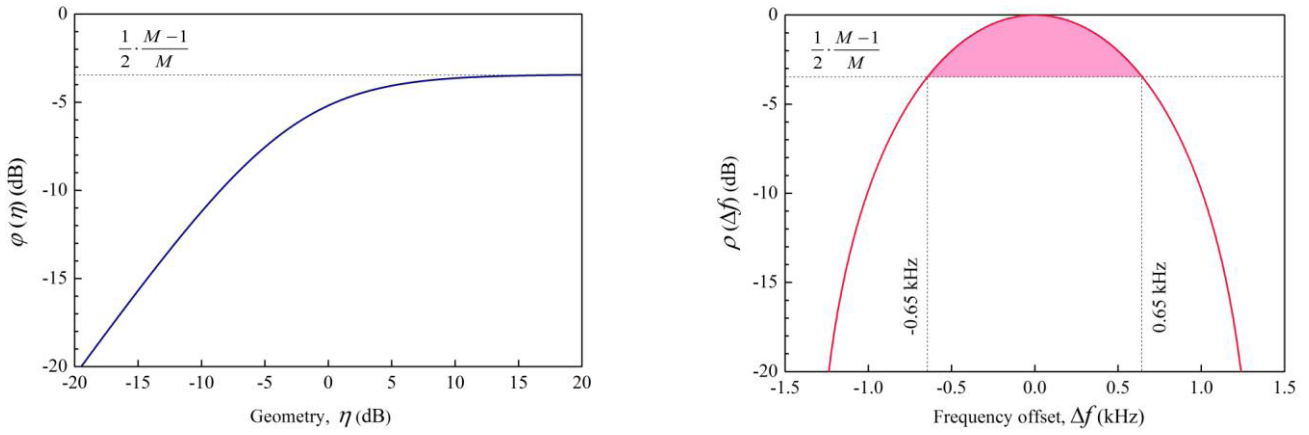

(a) (b)

FIGURE 6. (a) Plot of geometry factor $\varphi(\eta)$ in (25); and (b) plot of frequency offset factor $\rho(\Delta f)$ in (26).

whereas in the low geometry scenario, i.e., for the NB-IoT device with excessive penetration loss (e.g., deep inside a building, i.e., the basement) where $\eta \ll 5$ dB, we have

$$\lim_{\eta\to 0}\varphi(\eta) = \frac{M-1}{M}\cdot\eta \approx \eta, \tag{30}$$

which is close to the device's geometry. Since $\varphi(\eta)$ is a monotonically-increasing function of geometry η, the lower the geometry of the device is, the larger the attenuation to the differential detector SNR. For a device at $\eta = -19$ dB, the noise is boosted by a factor of ~19 dB (comparing to the matched-filter detector in the absence of frequency offset).

It becomes clear that, in general, the differential detector has no benefit when the frequency offset is small such that the geometry factor prevails over the frequency offset factor,

$$\varphi(\eta) < \rho(\Delta f), \tag{31}$$

i.e., the SNR attenuation caused by the noise amplification at geometry η is larger than the attenuation caused by the frequency offset (noting that a smaller value means a larger attenuation).

From (28), (31) holds as long as

$$\rho(\Delta f) > \frac{1}{2}\cdot\frac{M-1}{M}, \tag{32}$$

i.e., the degradation due to frequency offset is less than 3 dB or equivalently $|\Delta f| < 0.65$kHz (cf. Fig. 6 (b)), i.e., 0.65 ppm for 1-GHz carrier frequency, meaning that the geometry factor or the "noise amplification" effect is the dominant factor as long as $|\Delta f| < 0.65$kHz, as shown in Fig. 6 as well as Fig. 7. In other words, differential detector is not beneficial for frequency offsets less than 0.65 kHz, regardless of the device geometry η. However, when $|\Delta f| >$ 0.65kHz, differentiation can be beneficial depending on the device geometry, η.

There is a variant of the differential detection technique described in [24], in which the original waveform is pre-differentially-encoded sample-wise at the transmitter. This

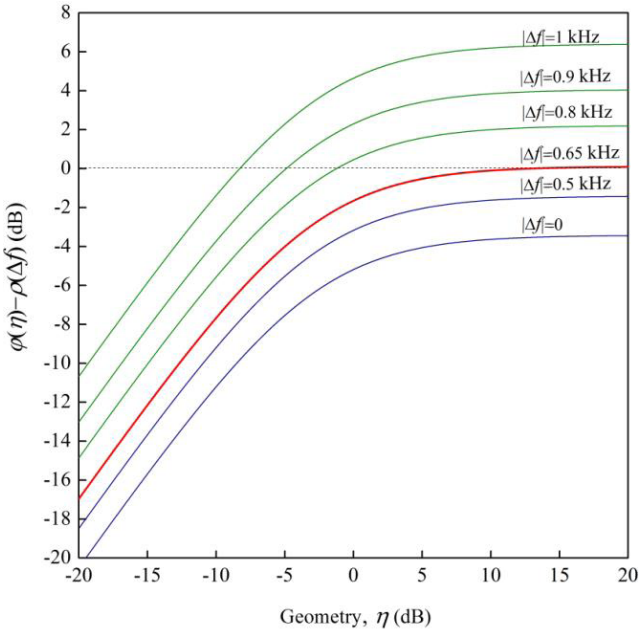

FIGURE 7. Plot of $\frac{\varphi(\eta)}{\rho(\Delta f)}$ in (24) as a function of the geometry η and frequency offset Δf.

pre-encoding requires the receiver to perform a differential decoding in order to preserve the same autocorrelation property of the original waveform, which leaves the matched-filter detection out of the option.

Finally, as a final note of this section, it is worth noting that in the practical detection, due to the limited sampling resolution, there exists a timing offset between the sampling point and the maximum correlation output time, which incurs additional loss to the detection energy. Fig. 8 plots the combined detection SNR loss due to the timing and frequency offset. It is observed that the matched-filter detector is more sensitive to not only the frequency offset but also the timing offset than the differential detector.

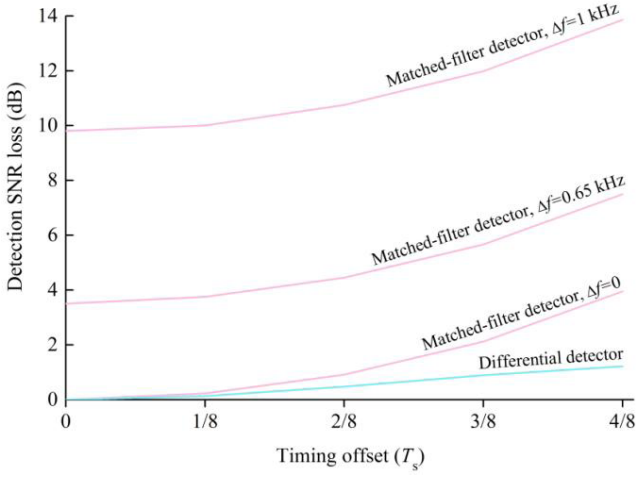

FIGURE 8. Plot of the combined detection SNR loss due to the timing and frequency offset, where T_s is the Nyquist sampling interval.

IV. DIFFERENTIAL AND MATCHED-FILTER DETECTION REGIONS

From the analysis in Section III, we conclude that (1) The performance of the matched-filter detector and differential detector depends on the device operating status, i.e., $(\eta, \Delta f)$, the oscillator accuracy and the geometry of the device in the cell; and

(2) The NPSS has the repetition structure which is facilitated to perform differential detection at the receiver, thereby providing the freedom in choice of a matched-filter detector or a differential detector according to the device operating status.

A natural question is then: What is the switching point or operating region that a differential detector outperforms a matched-filter detector? In this section, we use the analysis results from the previous section to derive the differential detection region and matched-filter detection region. Specifically, we look for

$$\Re^{\mathrm{DIF}} \triangleq \{(\eta, \Delta f) \,|\varphi(\eta) > \rho(\Delta f)\} \tag{33}$$

and

$$\Re^{\mathrm{MF}} \triangleq \{(\eta, \Delta f) \,|\varphi(\eta) < \rho(\Delta f)\} \tag{34}$$

where $\Re^{\mathrm{DIF}}$ is the region where the frequency offset factor dominates (i.e., $\varphi(\eta) > \rho(\Delta f)$), and hence the operating region for a differential detector, and $\Re^{\mathrm{MF}}$ where the geometry factor prevails (i.e., $\varphi(\eta) < \rho(\Delta f)$), and hence the region for a matched-filter detector. But first let us take a look at the geometry (η) properties in NB-IoT.

A. ANALYSIS OF DEVICE GEOMETRY IN NB-IoT

As earlier mentioned, the coupling loss of a device depends on the position in the cell, where the position farther away from the center (i.e., the low geometry) experiences higher coupling loss, and ergo low SNR. The maximum coupling loss for a traditional cellular system is ∼140 dB.

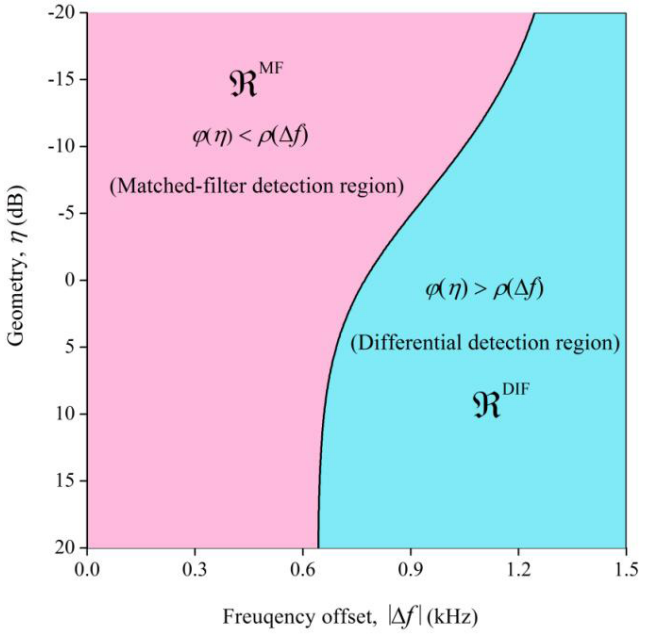

FIGURE 9. Plot of $\{(\eta, \Delta f) \,|\varphi(\eta) = \rho(\Delta f)\}$ in (36) that divides the NB-IoT device operating status into two regions according to the dominance of the two factors: the region $\Re^{\mathrm{MF}}$ where $\varphi(\eta) < \rho(\Delta f)$, i.e., the geometry factor prevails, so does the matched-filter detector ; and the region $\Re^{\mathrm{DIF}}$ where $\varphi(\eta) > \rho(\Delta f)$, i.e., the frequency-offset factor dominates, and the differential detector is superior.

However, there is a substantial NB-IoT use cases in which devices are deployed deep inside a building (e.g., the basement), which incurs an additional penetration loss of 20 dB.

To get an idea of a device's geometry in a typical mIoT system, assuming the transmit power allocated to the signal is p (dBm), and the maximum coupling loss is Δ (dB), the required receiver sensitivity is then $p - \Delta$ (dBm). If the bandwidth that the signal occupies is B (dB-Hz) and the noise figure of the receiver is δ (dB), the noise power at the receiver is thus $B + \sigma^2 + \delta$ (dBm), where σ^2 (dBm/Hz) is the noise power spectral density (i.e., −174 dBm/Hz). The corresponding geometry at the receiver is

$$\eta = (p - \Delta) - \left(B + \sigma^2 + \delta\right)(\mathrm{dB}). \tag{35}$$

For an NB-IoT system, the transmitter (base station) power p is assumed to be 35 dBm (for in-band and guard-band mode) and 43 dBm (stand-alone mode on the re-farmed GSM spectrum) [7]. We also assume that the maximum coupling loss is 144 dB (for a regular LTE deployment) plus 20 dB additional penetration loss in the mIoT environment (i.e., $\Delta = 144\mathrm{dB} + 20\mathrm{dB} = 164\mathrm{dB}$), the geometry η defined in (35) is −13dB for in-band and guard-band mode, and −5dB for standalone mode.

Since 20 dB is typically the highest geometry in a cellular macro cell, it is reasonable to assume that the geometry η for NB-IoT falls into the range from −13dB to 20 dB.

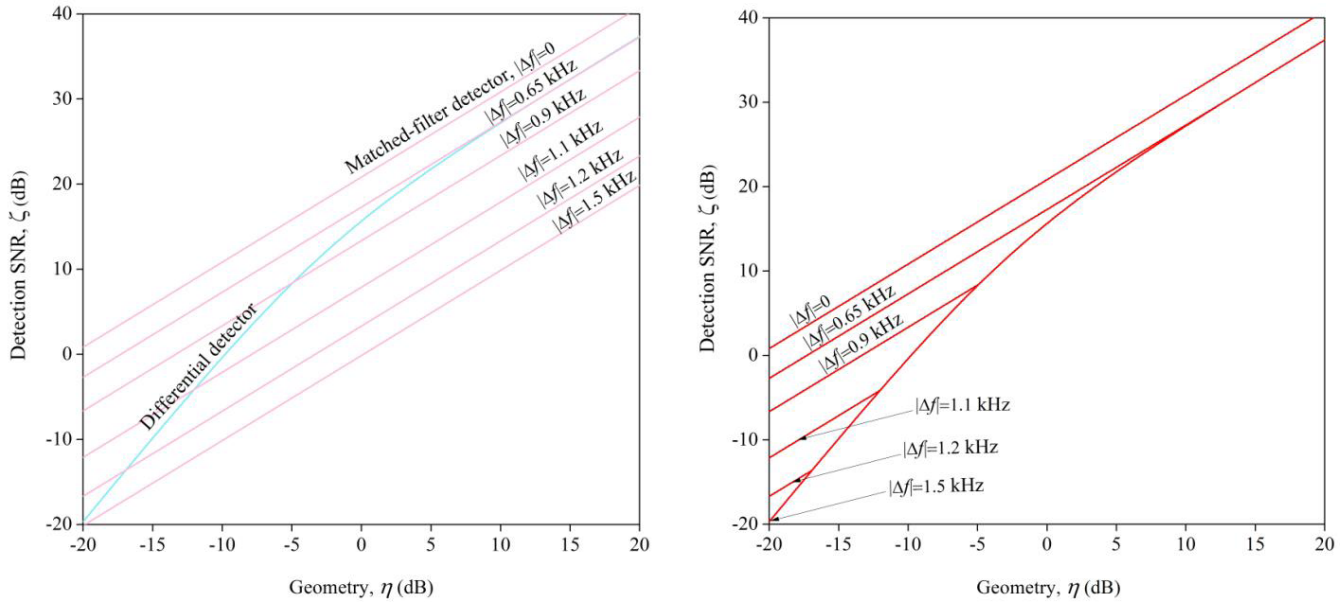

FIGURE 10. Plot of detection SNR ζ against geometry η at different frequency offset Δf : (a) for both matched-filter and differential detectors; and (b) for a selective detector which performs a selection between the two detectors according to the operating regions in Fig. 9.

B. OPERATING REGIONS

Based on the above analysis result, particularly the geometry factor and the frequency-offset factor that govern the detection performance, we are finally ready to derive the operation regions for a differential detector and a matched-filter detector.

Fig. 9 plots the "boundary" that separates the operation regions of the differential and matched-filter detectors, i.e., the set of device geometry and frequency offset pairs at which these two schemes share the same output SNRs,

$$\{(\eta, \Delta f)\,|\varphi(\eta) = \rho(\Delta f)\}, \tag{36}$$

with η in the range from -20 dB to 20 dB.

From the previous analysis, we know for a fact that

$$\varphi(\eta) < \frac{1}{2} \cdot \frac{M-1}{M}, \forall \eta. \tag{37}$$

As such, the matched-filter detector is guaranteed to outperform the differential detector as long as $\rho(\Delta f) > \frac{1}{2} \cdot \frac{M-1}{M}$. It is thus expected to see that,

$$\varphi(\eta) < \rho(\Delta f), \quad \forall \eta, \ |\Delta f| < 0.65\text{kHz}, \tag{38}$$

meaning that the matched-filter detector is superior at any device geometry for frequency offset less than 0.65 kHz. Hence, for a device with a quality oscillator or after frequency error has been compensated, the conventional matched-filter detector is more advantageous.

For higher frequency offsets (i.e., $|\Delta f| \gg 0.65$kHz), however, which factor prevails or which detector is advantageous depends on the device geometry. For example, the switch point at (-5dB, 0.9 kHz) in Fig. 9 indicates that the differential detector is beneficial for devices with a frequency offset larger than 0.9 kHz and geometry -5dB or higher. Similarly, (3 dB, 0.7 kHz) indicates a frequency offset of at least 0.7 kHz for devices at geometry 3 dB or higher to benefit. In general, high geometry and/or high frequency offset favor differential detection.

Fig. 10 plots the detection SNR ζ against geometry η at different frequency offset Δf, for (a) a matched-filter detector and a differential detector, and (b) a selective detector which applies a selection between the above two detectors according to the operating regions in Fig. 9.

C. IMPLEMENTATION EXAMPLE

A straightforward implication from the above results is that for a high-cost device (like the LTE UE for human-type communications or HTC) equipped with a temperature-compensated high-accuracy crystal, the geometry factor is typically a dominant factor, and a matched-filter detector is undoubtedly a first choice (which is in fact the case in HTC). For an NB-IoT device, neither the geometry factor nor the frequency-offset factor dominates in all scenarios, so neither matched-filter nor differential detector alone is the best solution. An NB-IoT device therefore needs the freedom in selecting the detector according to the frequency uncertainty and the geometry that it experiences, as shown in Fig. 11 (a). For devices with low crystal quality (large frequency uncertainty), the differential detector is a safer choice in the initial system acquisition.

Indeed, including both detectors at the receiver will increase the complexity. However, this increase can be minimized as both the detectors share one correlator, the local waveform/signal of which depends on the choice of the

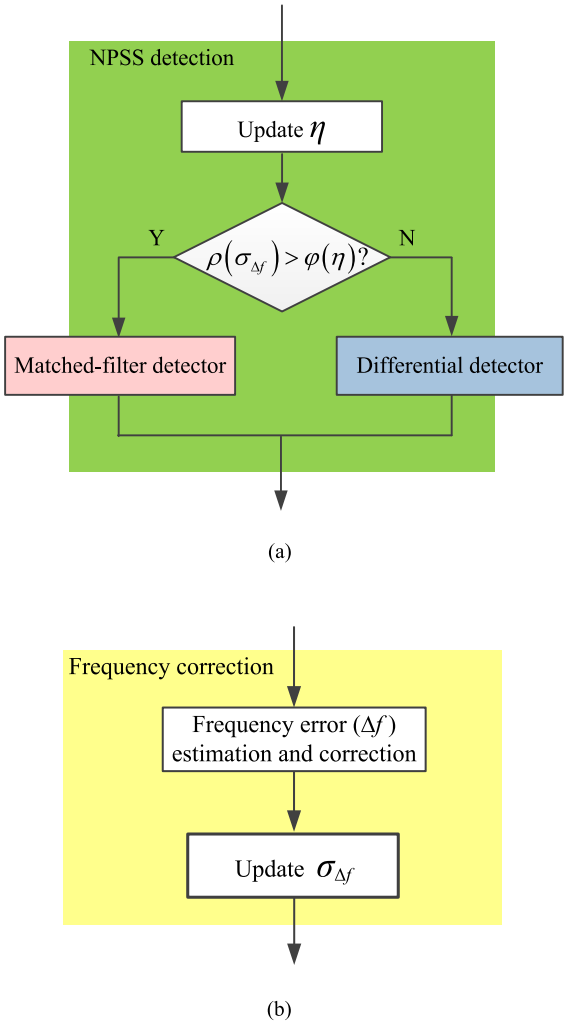

FIGURE 11. Schematic diagram to illustrate the implementation example of the selective NPSS detection based on the system acquisition procedure in Fig. 2.

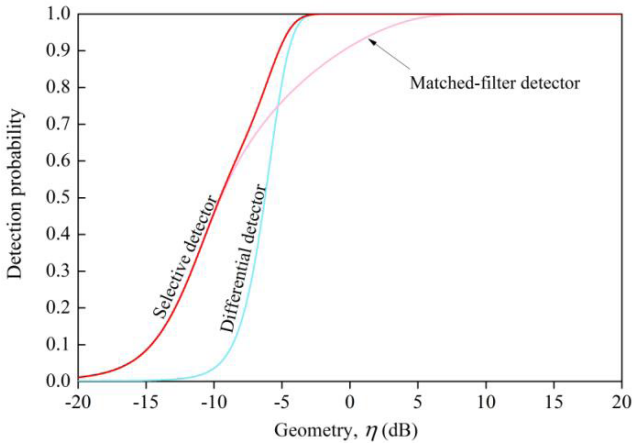

FIGURE 12. NPSS detection probabilities of a matched-filter detector, a differential detector, and a selective detector at various geometries, assuming the frequency offset of the device is uniformly distributed between −1.2 kHz and 1.2 kHz.

detector. For the matched-filter detector, it is the NPSS waveform, whereas for the differential detector, it is part of the received signal.

Although the frequency offset is difficult, if not impossible, to be completely corrected since different crystals have different stabilities and sensitivities to ambient temperature and other factors, the frequency uncertainty is converging to a certain degree (e.g., 1 ppm or 1 kHz at 1-GHz carrier frequency) each time when a device successfully acquires the system. In addition to making a frequency correction to the local crystal based on the acquired system frequency, the device collects and monitors the statistics on the crystal, e.g., the deviation of the crystal frequency, $\sigma_{\Delta f} \triangleq \sqrt{E\left(|\Delta f|^2\right)}$. It is updated after each successful acquisition: $\sigma_{\Delta f} = \alpha \cdot \Delta f + (1-\alpha) \cdot \sigma'_{\Delta f}$, where Δf is the frequency offset/error detected from the current acquisition, $\sigma'_{\Delta f}$ is the deviation estimated from the previous acquisition, and $0 < \alpha < 1$ is a constant, as shown in Fig. 11 (b). A device can then select the best detection scheme based on this statistic and its current geometry. Fig. 12 shows the performance of the selective detector under various geometries in comparison with the matched-filter and differential detectors.

V. CONCLUSION

In this paper, we study the detection performance of two detection techniques, i.e., a traditional matched-filter based detection and a differential detection. We introduce two factors: the geometry factor and the frequency offset factor. We show that, in general, the NPSS detection performance is governed by these two factors. That is, the performance of these two types of detectors depends on (1) the device geometry; and (2) its frequency offset from the network. When the geometry factor prevails, the matched-filter detector outperforms the differential detector; and when the frequency-offset factor dominates, the differential detector becomes advantageous. This indicates that the matched-filter technique (with a single template waveform) is no longer the optimal technique in the presence of a frequency offset between the transmitter and a receiver. To this end, a device requires having both techniques at its disposal, and the flexibility of selecting the right one depending on the actual operating conditions, i.e., the dominance of the two factors. This has the obvious advantage of enabling the receiving device to change the detector as needed to increase its tolerance to frequency offset (due to cost) and degraded SNR (due to coverage extension in NB-IoT). Specifically, based on the geometry and frequency offset factors, the operating conditions are divided into separate regions in each of which one detector works better than the other, such that the device can choose the detector accordingly and the immunity to both frequency offset and low signal quality is maximized, a challenging feat with low-cost crystals and extended coverage in NB-IoT. Finally, in the current study, the rectangular pulse is assumed for OFDM symbol. Different pulse shapes may affect detection

performance but is expected to be secondary to the effect of frequency offset. However, it is an interesting and valid topic for future study.

ACKNOWLEDGEMENT

The authors would like to thank the editor and the reviewers for their excellent comments that have greatly improved the presentation and the technicality of this paper.

REFERENCES

[1] H. Chaouchi, *The Internet of Things: Connecting Objects to the Web*. Hoboken, NJ, USA: Wiley, 2010.
[2] W. Yang *et al.*, "Narrowband wireless access for low-power massive Internet of Things: A bandwidth perspective," *IEEE Wireless Commun.*, vol. 24, no. 3, pp. 138–145, Jun. 2017.
[3] "Sigfox—One network a billion dreams," Sigfox, Labège, San Ramon, France, Whitepaper.
[4] N. Sornin, *LoRaWAN Specfication Ver. 1. 0*, LoRa Alliance, Tech. Rep., Jan. 2015.
[5] *3rd Generation Partnership Project Technical Specification Group Radio Access Network Evolved Universal Terrestrial Radio Access (E-UTRA) Physical channels and modulation (Release 13) Ver. 13.2.0*, document TS 36.211, Jun. 2016.
[6] Y. P. E. Wang *et al.*, "A primer on 3GPP narrowband Internet of Things," *IEEE Commun. Mag.*, vol. 55, no. 3, pp. 117–123, Mar. 2017.
[7] R. Ratasuk, B. Vejlgaard, N. Mangalvedhe, and A. Ghosh, "NB-IoT system for M2M communication," in *Proc. IEEE Wireless Commun. Netw. Conf. (WCNC)*, Doha, Qatar, Apr. 2016, pp. 1–5.
[8] N. Mangalvedhe, R. Ratasuk, and A. Ghosh, "NB-IoT deployment study for low power wide area cellular IoT," *Proc. IEEE 27th Annu. Int. Symp. Pers., Indoor, Mobile Radio Commun. (PIMRC)*, Sep. 2016, pp. 1–6.
[9] C. Bockelmann *et al.*, "Massive machine-type communications in 5G: Physical and MAC-layer solutions," *IEEE Commun. Mag.*, vol. 54, no. 9, pp. 59–65, Sep. 2016.
[10] A. A. Zaidi *et al.*, "Waveform and numerology to support 5G services and requirements," *IEEE Commun. Mag.*, vol. 54, no. 41, pp. 90–98, Nov. 2016.
[11] Z. Dawy, W. Saad, A. Ghosh, J. G. Andrews, and E. Yaacoub, "Toward Massive Machine Type Cellular Communications," *IEEE Wireless Commun.*, vol. 24, no. 1, pp. 120–128, Feb. 2017.
[12] C. Johnson, *Long Term Evolution in Bullets*. Northampton, U.K.: Createspace Press, 2012.
[13] M. Wang, A. Agrawal, A. Khandeka, and S. Aedudula, "Preamble design, system acquisition, and determination in modern OFDMA cellular communications: An overview," *IEEE Commun. Mag.*, vol. 49, no. 7, pp. 164–175, Jul. 2011.
[14] S. Ahmadi, *LTE-Advanced: A Practical Systems Approach to Understanding 3GPP LE Releases 10 and 11 Radio Access Technologies*. San Francisco, CA, USA: Academic, 2014.
[15] M. Hua *et al.*, "Analysis of the frequency offset effect on random access signals," *IEEE Trans. Commun.*, vol. 61, no. 11, pp. 4728–4740, Nov. 2013.
[16] M. Hua, M. Wang, K. W. Yang, and K. J. Zou, "Analysis of frequency offset effect on Zadoff-Chu sequence timing performance," *IEEE Trans. Commun.*, vol. 62, no. 11, pp. 4024–4039, Nov. 2014.
[17] S. Beyme and C. Leung, "Efficient computation of DFT of Zadoff-Chu sequences," *Electron. Lett.*, vol. 45, no. 9, pp. 461–463, Apr. 2009.
[18] F. Tufvsson, O. Edfors, and M. Faulkner, "Time and frequency synchronization for OFDM using PN-sequence preambles," in *Proc. IEEE Veh. Technol. Conf.*, vol. 4. Sep. 1999, pp. 2203–2207.
[19] J. Wang, Z. X. Yang, C. Y. Pan, M. Han, and L. Yang, "A combined code acquisition and symbol timing recovery method for TDSOFDM," *IEEE Trans. Broadcast.*, vol. 49, no. 3, pp. 304–308, Sep. 2003.
[20] H. Ni, G. Ren, and Y. Chang, "Complexity effective cell search scheme for OFDM cellular system," in *Proc. IEEE Int. Conf. Commun. Syst.*, Singapore, Nov. 2010, pp. 700–704.
[21] "NB-PSS and NB-SSS design 3GPP TSG RAN WG1 Ad-Hoc meeting," Qualcomm Incorporated, San Diego, CA, USA, Tech. Rep. R1-161981, Mar. 2016.
[22] C. R. Sheu and C. C. Huang, "A differential sliding correlation scheme for symbol timing detection in time domain synchronous OFDM systems," in *Proc. IEEE 69th Veh. Technol. Conf. VTC Spring*, Jun. 2009, pp. 1–5.
[23] H. Kroll, M. Korb, B. Weber, S. Willi, and Q. Huang, "Maximum-likelihhood detection for energy-efficient timing acquisition in NB-IoT," in *Proc. IEEE Wireless Commun. Netw. Conf. Workshops (WCNCW)*, Mar. 2017, pp. 1–5.
[24] *3rd Generation Partnership Project Technical Specification Group GSM/EDGE Radio Access Network Cellular System Support for Ultra Low Complexity and Low Throughput Internet of Things (Release 13) ver.1.0.1*, document TR 45.820, Mar. 2015.

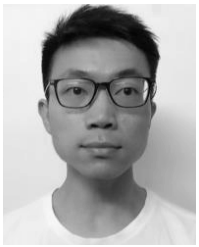

WENJIE YANG is currently pursuing the Ph.D. degree with the Nanjing University of Science and Technology, Nanjing, China. He is with the Wireless Networking and Mobile Communications Group, School of Electronic and Optical Engineering. His current research interests are in the areas of wireless communications and signal processing.

MIN HUA is currently pursuing the Ph.D. degree with the Nanjing University of Science and Technology, Nanjing, China. She is with the Wireless Networking and Mobile Communications Group, School of Electronic and Optical Engineering. Her current research interests are in the areas of wireless communications and signal processing.

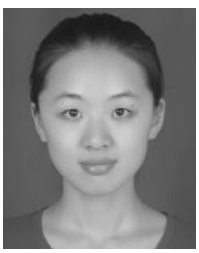

JINGJING ZHANG is currently pursuing the Ph.D. degree with the Nanjing University of Science and Technology, Nanjing, China. She is with the Wireless Networking and Mobile Communications Group, School of Electronic and Optical Engineering. Her current research interests are in the areas of wireless communications and signal processing.

TINGTING XIA is currently pursuing the Ph.D. degree with the Nanjing University of Science and Technology, Nanjing, China. She is with the Wireless Networking and Mobile Communications Group, School of Electronic and Optical Engineering. Her current research interests are in the areas of wireless communications and signal processing.

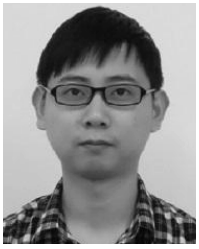

JUN ZOU received the Ph.D. degree with the Wireless Networking and Mobile Communications Group, School of Electronic and Optical Engineering, Nanjing University of Science and Technology, Nanjing, China. Since 2016, he has been with the Wireless Networking and Mobile Communications Group, Nanjing University of Science and Technology, where he is currently a Lecturer at the School of Electronic and Optical Engineering. He has over ten IEEE journal publications. His research interests are in the areas of wireless communications, signal processing, and Internet of Things.

CHENGLING JIANG received the Ph.D. degree from the School of Electronic and Optical Engineering, Nanjing University of Science and Technology, Nanjing, China. Since 2013, he has been with the Information and Telecommunication Branch, State Grid Jiangsu Electric Power Company. His research interests are in the areas of private wireless communications and networking for power networks.

MAO WANG received the Ph.D. degree in electrical engineering and computer science from the University of Kentucky, Lexington, KY, USA. He is currently a Professor with the National Mobile Communications Research Laboratory, Southeast University, Nanjing, China. He is also an Adjunct Professor with the School of Electronic and Optical Engineering, Nanjing University of Science and Technology, where he is the Director of the Wireless Networking and Mobile Communications Group. He holds over 90 U.S. patents and has over 30 IEEE journal publications. His research interests include communication theory and wireless networking.